Wick action in mature mortars with binary cements containing slag or silica fume – The relation between chloride and moisture transport properties under non-saturated conditions.

Nilla Olsson[1,2*], Fatmawati Abdul Wahid[3], Lars-Olof Nilsson[1], Charlotte Thiel[4], Hong S. Wong[3] and Véronique Baroghel-Bouny[2]

[1]Lund University, Division of Building Materials, Lund, Sweden

[2]Paris-Est University, IFSTTAR, Materials Department FM[2]D laboratory, Marne-la-Vallée, France

[3]Concrete Durability Group, Department of Civil and Environmental Engineering, Imperial College London, UK

[4]Technical University of Munich, Center for Building Materials, Munich, Germany

* Corresponding author. E-mail address: nilla.olsson@byggtek.lth.se. Full postal address: Nilla Olsson, Division of Building Materials, Lund University, P O Box 118, 221 00 Lund, Sweden. Tel: +46-705-79 85 15

Abstract

Moisture and ionic transport under non-saturated condition is an important, but poorly understood transport phenomena particularly for mature systems containing supplementary cementitious materials. This paper investigates the moisture and chloride profiles of 3-year old mortars containing Portland cement (OPC), slag and silica fume (SF) after long-term (30-48 months) wick action exposure in 1.09M NaCl solution. Moisture profiles were measured with ^{1}H NMR relaxometry and chloride profiles with microXRF. The measured profiles were

discussed in relation to moisture dependent material properties such as chloride diffusion coefficients, moisture diffusion coefficients, and desorption isotherms. Results show that the combination of different cementitious materials, e.g. the cementitious binder, is the key factor affecting chloride penetration depth. The cementitious binder also strongly affects chloride diffusion coefficient, moisture diffusion coefficient and chloride binding properties, which are all important parameters for the prediction of chloride ingress.

Keywords:

Transport properties (C); Durability (C); Chloride (D); Microstructure (B); Long-Term Performance (C).

1 Introduction

Transport of moisture and ionic species are closely related to degradation of concrete structures [1]. These topics have been widely investigated under saturated conditions. But in many applications, the deterioration process occur under unsaturated conditions, where the transport of ions and moisture are coupled. However, unsaturated transport is rarely studied experimentally, partly because of the complex moisture dependency and difficulties in decoupling ionic transport from moisture transport. Fundamental understanding of this is absolutely critical, for example in advancing service-life prediction models for structures in realistic exposure environments.

A method to study the interaction between moisture and ion transport is through wick action experiments [2]. Wick action is the transport of a solution (ionic solution or pure water) through a material, where one surface of the material is in direct contact with the solution and the opposite surface is exposed to a drying environment. If the relative humidity (RH) on the dry side is constant, the rate of absorption on the wet side will be similar to the rate of evaporation on the dry side when steady-state conditions are reached. If the experiment is performed with pure water, the moisture profile will hereafter be constant, and be dependent on the moisture diffusion coefficient and moisture sorption properties of the material.

Commonly in wick action experiments, the water contains ionic species which are transported with the moisture through the material. The ionic species will penetrate and precipitate either within the specimen, or at the surface of the specimen exposed to a drying environment, depending on the composition of the material and of the environmental conditions. In these cases, there is convective transport of ions with moisture transport, but also pure diffusive transport due to gradients in ionic concentration. Therefore, both the moisture diffusion coefficient and ion diffusion coefficient are important material properties for prediction of the ion profile through a structure [3]. The convective transport of ions with moisture transport is often regarded as the governing transport mechanism in cementitious materials, and pure ionic diffusion is assumed to be of minor importance [3-5]. This assumption has shown to be efficient for prediction of ion profiles for materials with a clear convective moisture transport and a moisture dependency in moisture transport [3]. However, the approach has limited abilities to predict the ion distribution for denser materials with limited or no moisture dependency in moisture transport, such as cementitious materials at low water to binder ratio (w/b) or containing supplementary cementitious materials (SCMs) [6]. The interaction and

binding of the ionic species with the solid phases in cementitious materials, and the RH on the dry side of the specimen, will also affect the ion profile [2].

Tuutti [7] made an early investigation of wick-action in cementitious materials. He discussed chloride concentration profiles in relation to w/b and drying condition for mortars with OPC and slag. It was concluded that ion transport in slag blends is less sensitive to w/b than mortars with OPC. Buenfeld et al [2] made another early investigation of OPC mortars after 9 months wick action exposure. They included modeling of the obtained chloride profiles from measured material properties. However, the modeling was based on ion transport only with liquid moisture transport and does not take into account the diffusive ion transport and the moisture dependency of the chloride diffusion coefficient. This approach produced reasonable prediction of ion transport for OPC mortars with high w/b. But for denser materials with little or no liquid moisture transport, the diffusive ion transport and its moisture dependency need to be considered for accurate prediction of the ion profile. A more recent model [4] includes the diffusive transport of ionic species, but the ion diffusion coefficient was related to tortuosity of the liquid phase, which is problematic when modeling dense materials. In Baroghel-Bouny et al [3], the measured ion profiles from wick action experiment by Francy [5] were predicted through a model that relates ion diffusion coefficient to the degree of saturation of the material. It was concluded that an accurate assessment of diffusive ion transport is crucial to achieve an accurate prediction of ion distribution in cases where liquid moisture transport is low. However, such data are rare. The need for more experimental research on unsaturated transport has been highlighted in a recent review [8], and in particular the effect of SCMs on transport properties.

In two recent publications by Olsson et al [9] and Olsson et al [6], the moisture dependency of ion diffusion and moisture transport properties for mortars with slag or silica fume (SF) were investigated. In this paper, measured moisture and chloride ion profiles after wick-action exposure of the same mortars are presented. The profiles are discussed and related to w/b, cementitious binder, drying conditions, and material transport properties such as ion diffusion coefficient, moisture diffusion coefficient and desorption isotherm of the mortars. The overall aim is to enhance the understanding of key parameters influencing non-saturated chloride transport under wick action in cementitious materials containing SCMs.

2 Materials

In this study, four binders and two w/b were investigated. The investigated binders were ordinary Portland cement CEM I 42.5N (OPC), OPC with 5% silica fume (SF), and OPC with 40% or 70% ground granulated blast furnace slag (slag), respectively (all by mass). These binders were used to produce mortars with siliceous sand (CEN-Standard Sand according to EN 196-1) of particle sizes 0-2 mm, at w/b 0.38 and 0.53. To get similar initial capillary volume in all systems, the exact w/b was calculated to obtain equivalent volume of paste in relation to the volume of water for all mortar mixes. This gave a slight variation in w/b due to differences in density between the OPC, SF and slag. A small amount of plasticizer (~ 1 kg/m^3) was used in the w/b 0.38 mortars to improve workability. The composition of mortars and binders are given in Table 1 and Table 2, respectively.

The mortars were batched in a pan mixer and cast as blocks (600 x 250 x 250 mm^3) in wood molds, and compacted with a vibrating rod. The blocks were demolded after 24 h and put into

sealed containers with a limited amount of tap water for wet curing. The blocks were immersed in approximately 1 cm of water to limit the amount of water to minimize leaching. Cores of 94 mm diameter were drilled horizontally using a diamond corer through the blocks at the age of 7 days. The cores were immediately placed back into their holes in the blocks for further wet curing. The reason for keeping the samples in their blocks was to limit direct exposure to water and therefore leaching. After three years of curing, the cores were cut into discs with thickness of 35 mm and again placed back into their blocks. The material used in this study was taken from the same blocks as those in previous studies [6, 9, 10], and was therefore expected to have similar properties. However, the difference in age between studies will affect the properties.

3 Methods

3.1 Wick-action exposure

In the wick-action experiment, disc specimens were exposed to 1.09 M (6% by mass) sodium chloride solution on one flat end of the disc, and to air at controlled relative humidity (RH) on the opposite end. Two RHs were used, 33% and 75%, which were generated by using saturated salt solutions of magnesium chloride (33% RH) and sodium chloride (75% RH) [11]. The air was circulated with a fan and the RH was regularly validated with RH sensors. The experiment was performed in sealed boxes at a temperature of 20 ºC ±0.5 ºC, and with a carbon dioxide absorbent to avoid carbonation of the material.

The exposure to 1.09 M NaCl solution was carried out by mounting the flat end with a glass cup of similar diameter as the disc specimen, viz. 95 mm. The glass cups were filled with NaCl solution and the edge sealed with butyl tape to prevent side leakage. The cups were placed upside down in sealed boxes so that the NaCl solution was in contact with the top flat surface of the disc specimen. The specimens for wick-action exposure were taken from the blocks one month after cutting, i.e. at an age of approximately three years.

3.2 Chloride profiles from microXRF

The specimens were exposed to wick-action for 30 months prior to ion profile determination. The weight of the cups was determined regularly to ensure that a steady-state flux was achieved during the exposure period. At the end of the exposure period, the glass cups were removed, and the specimens were split along the diameter with a wedge split. This method was considered to have the least risk of affecting the ion distribution on the analyzed surface. The two halves were assembled back together, wrapped in plastic sheets to prevent drying and stored for one to two weeks prior to micro X-ray fluorescence (microXRF) analysis. The effect of surface roughness is investigated in the work of Abdul Wahid [12]. This investigation, in combination with the fact that all samples were analyzed similarly, justifies comparison between profiles.

Chloride profiles were measured using an Orbis PC energy-dispersive microXRF system by Edax-Ametek. The microXRF is equipped with an 80 mm^2 Si(Li) detector with Be window for analysis of Na to U, and a motorised stage with 5 ± 2 µm minimum step size. Analysis was carried out using a 2 mm spot size at 20 kV beam voltage, 30% dead time, 100s live

acquisition time and 25.6 µs time constant. More crucially, the analysis was carried out in an ambient environment (i.e. no vacuum) to prevent drying of the specimen that would otherwise influence the measured profiles. A 25 µm aluminium filter was employed to improve the detection of chlorine by removing overlapping rhodium spurious peaks.

In total 20 profiles were measured; one profile for each mortar and wick-action exposure condition (75% or 33% RH), i.e. 16 profiles, and a replicate analysis in 4 cases. The freshly split surface of each specimen was analyzed directly without any polishing or drying of the specimen to avoid re-distribution of chlorides. A spot size of 2 mm was chosen to ensure a substantial volume of analyzed material to obtain representative composition of the mortar. Analysis was carried out starting from the wet face exposed to NaCl, and then at every 2 mm depth increments ending at the dry face. Ten spot measurements were made at each depth increment and the results averaged. A total of 170 spots were analyzed per sample, covering an area of approximately 680 mm^2, to construct one profile. For each spot, the measured characteristic X-ray spectrum was processed for background substraction to obtain the net intensity (counts per second) for chlorine, which was then normalized to that of calcium. Further details of the microXRF analysis are given in Marin-Cudraz (2015) [13] and Abdul Wahid (2017) [12].

3.3 Total chloride content from cut slices

The specimens were also analyzed to obtain the total chloride content at some selected depths. Chloride content was determined as the mass fraction of total chloride per mass of binder. Slices were cut at the selected depths. The thickness of the slices varied slightly and the exact

thickness of the slices were measured individually, and are shown in the results. The results represent single measurements. The slices were then ground to powder and dissolved in nitric acid with concentrations 0.057 M. Chloride content was measured with an ion-selective electrode (ISE), and the binder content was calculated from the CaO content determined by titration. The buffer solution contained 1.6 M KNO3, 1.0 M CH_3COOH and 1.0 M $NH_4CH_3CO_2$.

3.4 Moisture profiles from ^1H NMR relaxometry

Parallel specimens were exposed to wick-action for 48 months and then analyzed to determine moisture profiles. At the end of the exposure period, the glass cups were removed, and the wet surface was covered with a cloth with exposure solution and sealed. The specimens were then wrapped in plastic sheets and stored up to two months prior to analysis.

Several methods for determination of moisture profiles were evaluated before the selection of ^1H NMR relaxometry at TU München. X-ray absorption measurements and ^1H NMR relaxometry at another lab were evaluated, but these attempts did not give sensible results. Due to lack of specimens, only 10.5 unique profiles were measured and reported here. The measurements were carried out with an NMR MOUSE PM 25 from Magritek [14]. The sensitive volume of each measured depth was 30 x 30 x 0.2 mm^3. A motor step of 0.2 mm was used to a total depth of 9.6 mm from each side of the specimen. The measurements were also performed to a total depth of 19.6 mm, but the scatter turned out to be too large due to poor signal-noise ratio, and these results were therefore excluded from the analysis. T_2

measurements with a CPMG sequence (256 scans and 256 echoes) were performed with a repetition time of 500 ms.

The signal amplitude obtained during the measurements is directly proportional to the total content of free and physically bound water (the device neither detects water in the form of vapor nor chemically bound water). However, the proportionality is different depending on RH and the sensitivity to moisture corresponding to an RH below some 75 % is low. The signal amplitude decreases slightly with increasing distance from the magnetic field. To overcome this issue, the results were corrected for the variation of the recorded signal with depth. The correction factor was calculated from a measurement similar to the measurements on mortar specimens, but performed on a container with pure water. The measurement was replicated four times and an average of the four measurements was used for calculation of the correction factor. The NMR measurements were carried out from both end surfaces of the specimens to a total depth of 9.6 mm from each end, therefore the center portion ~ 15.8 mm could not be analyzed.

Another correction applied to the results was the removal of positions not completely inside the specimens due to surface roughness and wrapping in cling film during the measurement. At motor position 0 mm from the wet side of the specimens, the first four positions had very low intensity compared to subsequent positions. Therefore, the first four data points were regarded as measurements in air and were excluded from the data analysis. On the dry side of the specimens however, it was more difficult to judge which position is the first value completely within the specimen due to the low RH. Therefore, the same number of points as on the wet side, i.e. the first four positions, was removed from the results from the dry side. In

addition, it has to be kept in mind that magnetic and paramagnetic compounds inside the material can lead to a shift in the measured signal. Therefore, the water content is slightly overestimated for cementitious materials. Due to the high Al_2O_3 content, this effect is even more pronounced for the binders with slag. To take this into account calibration measurements are necessary to obtain fully quantitative results [15].

4 Results and Discussion

4.1 Chloride profiles

Fig. 1 a)-d) shows the measured chloride content profiles determined with microXRF. Note that the results are expressed as total Cl/Ca ratio and different scales were used on the vertical axis for clarity. Error bars represent +/- one standard error of the average. Major differences in chloride profiles can be identified between the four binders. Fig. 1 a) shows that for the control OPC mortars, chlorides have penetrated through the specimen thickness and in some cases, have begun to accumulate near the surface exposed to low RH. Details of the chloride profiles close to the surface at 35mm in Fig. 1 a) are shown in Fig. 2. It can be seen that OPC 0.53 – 33% RH showed the highest chloride accumulation near the dry surface, followed by OPC 0.53 – 75% RH. In contrast, OPC 0.38 showed relatively less accumulation of chloride. Therefore, the amount of chloride ingress and accumulation increased with increase in w/b and drying severity, as expected. However, the very high levels measured in the first 12 mm of OPC 0.53 – 75% RH was unusual and probably due to side leakage caused by failure of the butyl tape.

For mortars containing slag or silica fume, Fig. 1 b)-d) show that their chloride concentrations and penetration depths are much smaller compared to the control OPC mortar, and that no significant accumulation of chlorides have started near the face exposed to lower RH. Overall, the 70% slag mortar was more resistant to chloride ingress compared to the 40% slag and 5% SF mortars on the basis of penetration depth. Samples with slag also showed higher chloride content at the exposed surface, due to the effect of chloride binding that increases in SCMs that contain high alumina content. The chloride content dropped quickly with depth because of the high resistance to chloride ingress. Mortars with lower w/b tended to show marginally less chloride penetration, but this was not observed consistently. Therefore, it seems that w/b has a relatively smaller influence on chloride ingress in wick action than the type of binder in mature blended mortars, probably because of the extensive SCM reaction that densifies the pore structure. Furthermore, the profiles for 70% slag 0.38 at 33% RH and 75% RH displayed an anomaly in that a small increase in chloride intensity was observed after the first minimum at 15 mm, which is likely caused by an experimental error.

A number of replicate chloride analyses were carried out. Generally, these show reasonably good agreement for example OPC 0.38 – 33% RH and 40% Slag 0.38 – 33% RH. However, other samples such as 5% SF 0.38 – 33% RH and 70% Slag 0.38 – 33% RH showed slightly larger variation between replicates. This could be due to the fact that the microXRF analyses were carried out under ambient pressure and on fractured sample as-is without further treatment, which are non-optimal conditions. Analyses in vacuum and on flat polished surface will improve signal-to-noise ratio and produce more repeatable results, but re-distribution of chlorides is likely to occur during sample pre-drying and grinding. Another possible reason is the presence of imperfections and compaction voids in the specimens, which also exist in real concrete structures. For example, it has been shown that empty air voids act as insulators for

moisture transport while water-filled air voids act as conductors, and a difference of 1% air content can alter transport by 14% in total [16]. This difference should affect ion transport similarly. Furthermore, microcracks can form during drying and sample coring. It has been shown in recent experimental and numerical studies that these microcracks have a significant influence on transport processes [17, 18].

The results from this study suggest that for specimens that have been well-cured prior to exposure to chloride wick action, the differences in binder type between specimens induce a larger effect on chloride penetration than the investigated w/b (0.53, 0.38) and the RH (75%, 33%) on the dry side of specimen. Significant differences in chloride penetration depth can be identified between the different binders and therefore, it can be concluded that the cementitious binder is the major factor affecting chloride transport in unsaturated condition during wick-action exposure.

4.2 Chloride profiles related to material properties

The chloride profiles can also be discussed in terms of other material properties, such as moisture diffusion coefficient, desorption isotherm, chloride diffusion coefficient, and chloride binding capacity. Two recent publications [6, 9] investigated material properties for the same mortars as in this study. Fig. 3 a)-b) is taken from [6] and shows the moisture dependency of the moisture diffusion coefficient. The measurements were performed at an age of two years. The moisture diffusion coefficient is constant at low RH for all mortars. At higher RH, the OPC and 5% SF 0.53 mortars show a clear moisture dependency in the moisture diffusion coefficient, whereas the others do not. In the interval where the moisture

diffusion coefficient is constant, the mortars with higher w/b have larger moisture transport. Fig. 4 is also taken from [6] and shows the desorption isotherms for the mortars in this study. Compared to the large differences in moisture transport between the mortars, the moisture content shown by the desorption isotherms is of similar order of magnitude. However, large differences can be found by comparing specific RH intervals, e.g. from 80% to 97% RH. In this RH interval, the moisture content of 70% slag 0.38 increased by only 8 kg/m^3 whereas OPC 0.38 increased by 29 kg/m^3. The measurements were performed at an age of four years.

Fig. 5 is taken from [9] and shows the moisture dependency of the chloride diffusion coefficient. All mortars show a clear moisture dependency in chloride diffusion. The mature slag mortars have the lowest chloride diffusion while the OPC mortars the highest. These measurements were performed at an age of about one year. The properties of the mortars shown in Fig. 3 a)-b), Fig. 4 and Fig. 5 can be related to their performance in wick-action experiment from this study.

Fig. 6 shows the total chloride content measured with profile grinding. The total chloride content at 0 mm gives an indication of the chloride binding potential of the different binders when in contact with the NaCl-solution. The 70% slag mortar has the highest total chloride content followed by the 40% slag and 5% SF, while the OPC mortars has the lowest total chloride content. It should be pointed out that these results are consistent with the chloride profiles obtained from microXRF in Fig. 1 c)-d) where the 70% slag and 40% slag mortars showed the highest surface chloride content and steepest chloride gradient near the surface region. The same applies for the 5% SF mortar as shown in Fig. 1 b) where the surface

chloride content and gradient are lower compared to the slag mortars, and therefore the impact of chloride binding is expected to be smaller.

From the material properties discussed above in this section, it can be concluded that the OPC mortars are expected to have the largest chloride penetration depths, which agrees with the measured chloride profiles in Fig. 1. The OPC mortars have the highest chloride diffusion coefficient in all RH intervals, and also the highest moisture diffusion coefficient in the RH interval 100% to 70% RH. They also have a clear convective moisture transport in this RH interval that will accelerate chloride penetration. These mortars also have the lowest total chloride content at the surface, which means the lowest chloride binding, and this enables a higher penetration rate.

The results in Fig. 1 also show that the mortars with 5% SF binder have the second largest chloride penetration depths, followed by the mortars with 40% slag and 70% slag. This order of penetration depths agrees well with the total chloride content shown in Fig. 6, which provides an indication of the chloride binding capacity for the different binder types. As discussed previously, a larger chloride binding capacity will increase the surface chloride content and retard the chloride ingress to a larger extent.

The correlation between chloride profiles to other material properties is not as clear as the correlation to chloride binding capacity. It seems that the chloride penetration depths do not show strong correlations to neither the chloride diffusion coefficient nor the moisture diffusion coefficient. From Fig. 5, the variation in chloride diffusion coefficient between w/b appears to be larger than that between binders. All mortars at w/b 0.38 except OPC have

similar chloride diffusion coefficient of approximately $0.8 \cdot 10^{-12}$ m^2/s at 100% RH. These mortars also share similar chloride diffusion coefficient at lower RH. This observation is also valid for w/b 0.53, but here the chloride diffusion coefficient is around $1.3 \cdot 10^{-12}$ m^2/s at 100% RH. Similarly, there appears no obvious relation between chloride penetration depth and moisture content. However, it needs to be kept in mind that these material properties and the chloride profiles were measured at different ages.

Fig. 3 suggests that w/b ratio has a greater effect on moisture diffusion coefficient compared to cementitious binder for the slag and the 5% SF mortars. Interestingly, the 5% SF mortar at w/b 0.53 shows a clear moisture dependency in moisture diffusion coefficient whereas the mortar at w/b 0.38 does not. The corresponding ion profiles in Fig. 1 b) show that this could possibly be an important factor. The average chloride penetration for w/b 0.53 is clearly deeper than that for w/b 0.38. This suggests that the moisture dependency of the moisture diffusion coefficient could be a key parameter for predicting chloride penetration depth. However, more replicate measurements would be needed to confirm this.

In conclusion, it seems that the effect of chloride binding becomes increasingly important when the moisture diffusion coefficient is low and the total ion transport is dominated by ionic diffusion. However, the difference in penetration depths between OPC and 5% SF mortars cannot solely be explained by differences in binding. Here, it seems that the difference in chloride and moisture diffusion coefficients are of larger importance. A large moisture dependency of the moisture transport coefficients means that a larger portion of the ion transport is due to convection, which enables this mechanism to be predominant for the chloride penetration depth.

4.3 Moisture profiles

Fig. 7 a)-g) shows the results from NMR measurements of moisture profiles presented as intensity of the NMR signal (in arbitrary units). These results are corrected for the decrease in recorded signal with increasing depth in the sample, using the correction factors shown in Fig. 8 that were obtained using the method described in Section 3.4. Fig. 9 from Rucker-Gramm [19] shows the variation in intensity with moisture content in concrete. This figure was obtained from calibration measurements on samples conditioned to a series of RH. These measurements were performed on an OPC mortar with w/b 0.6. The moisture content will vary between mortars, but the sensitivity of the ^{1}H NMR for moisture in different pore sizes should be similar. Since the NMR signal is sensitive to the state of the water (^{1}H) within the pore structure, the recorded signal is not linearly proportional to water content in cementitious materials because a large portion of the water is present in small pores where its interaction with the pore wall limits mobility and therefore the signal intensity recorded during NMR measurements. Fig. 9 shows that only small changes in intensity are recorded for water present in pores smaller than around 2.5 nm, which represent the pore size filled at 65% RH. Beyond this value, the recorded intensity increases significantly and has an approximate linear relationship with increase in moisture content.

The effect shown in Fig. 9 needs to be kept in mind when analyzing the results in Fig. 7 a)-g). In all cases, Fig. 7 a)-g) shows very high NMR signal intensity on the wet side in the first 0-3 mm. This is interpreted as free water in large air voids, for example compaction voids, which have been filled during the long exposure period. After this peak there is a plateau, representing the moisture content at capillary saturation. In Fig. 7 a), b) and d), this plateau

continues all the way through the sample. This does not seem to agree with what is expected from the moisture diffusion coefficients in Fig. 3 and the desorption isotherms in Fig. 4 that suggest that moisture content should decrease from the wet surface to the dry surface. However, it should be borne in mind that these properties were measured with pure water, while the moisture distributions in Fig. 7 relate to NaCl in pore solution [20]. For the specimen in Fig. 7 a), salt and moisture were visually observed on the dry side prior to NMR analysis. For the specimens in Fig. 7 b) and d), precipitation was not observed on the surface, but their ion profiles suggest that ions have started to accumulate just beneath the surface. It should also be noted that the chloride profiles in Fig. 1 were measured 18 months prior to the moisture profiles. Therefore, chloride ingress would continue to increase during the additional 18 months period and accumulation of chloride close to the dry surface would affect the moisture distribution obtained from NMR.

In Fig. 7 c) and e)-g), parts of the specimens show a similar plateau as in Fig. 7 a), b) and d), indicative of capillary saturation within this region. However, the recorded intensity starts to decrease towards the surface exposed to lower RH. In the experimental set-up with 75% RH on the dry side, the recorded intensity can be regarded as proportional to moisture content since Fig. 9 indicates a linear relationship at the 75-100% RH interval. However, for specimens with 33% RH on the dry side, the intensity profile is not proportional to moisture content in the material.

To visualize the effect of the non-linear relation between intensity and moisture content in the material, an example is made for one of the mortars, shown in Fig. 11. Here the general calibration curve shown in Fig. 9 is used in combination with quantitative data from the

desorption isotherm in Fig. 4. The relevant points in Fig. 9 are marked in Fig. 10 and Fig. 11. From the desorption isotherms for the mortars shown in Fig. 4 and the exposure conditions, the moisture content in three points is known; at capillary saturation, at 75% and at 33% RH. These are noted in Fig. 11 with green points circled in black. The aim of Fig. 11 is to visualize a more realistic shape of the profile in moisture content for the specimens with 33% RH on the dry side.

The visualized moisture profile in Fig. 11 is estimated from the measured intensity on the dry side at 75% RH, I(75%). This intensity is marked on the intensity profile for the specimen with 33% RH on the dry side. From this point, the profile is fitted to a linear fit to the point on the y-axis representing the moisture content at 33% RH, w(33%). A difficulty with this estimation of the moisture profile is that it is very sensitive to the lowest measured point in the profile with 75% RH, I(75%), on the dry side. A small uncertainty, or shift in I(75%) up or down, effects the shape of the estimated moisture profile significantly. Therefore it is not fruitful to analyze the results based on these profiles in more detail. However, it is an important observation since it explains why the measured intensity on the dry side of specimens is similar even though the exposure in RH is different, i.e. 33% vs 75% RH.

4.4 Interaction between moisture profiles and chloride profiles

The presence of ions in the exposure solution and pore solution complicates the relation between moisture profiles and microstructural properties. For example, the desorption isotherms, and thereby the moisture diffusion coefficient with RH as potential, will be affected by the increased ionic strength of the pore solution when the NaCl-solution is

transported through the specimens. The desorption isotherms will also shift to the left and the pore structure will be capillary saturated at humidity levels lower than 100% RH.

The moisture and chloride profiles for OPC mortars can be related to the changes in the desorption isotherms with chloride concentration. All chloride profiles for OPC mortars in Fig. 1 a) and Fig. 2 show a small increase in chloride content from the wet surface at 0 mm to the surface exposed to lower RH at 35 mm. This increase is also detected in the chloride profile determined from titration for the OPC mortar shown in Fig. 6. The corresponding moisture profile in Fig. 7 a) also shows a possible increase in moisture content towards the surface exposed to lower RH, especially from about 30 to 35 mm, where the highest chloride concentrations also are found. This suggests that accumulation of salts in large air voids affects the total moisture content, which may increase above the level of capillary saturation.

Another observation from Fig. 1 b)-d) is the tendency for the chloride profiles to have a convex shape. As seen in Fig. 3 a)-b), the mortars with slag and the mortar with 5% SF w/b 0.38 have no moisture dependency in the moisture diffusion coefficient, and a low total moisture transport in all RH intervals. For these mortars, the governing transport mechanism for chloride ingress is diffusion. The moisture dependency of the chloride diffusion coefficients is one factor that contributes to the convex shape of the chloride profiles. It can be deduced from the moisture distributions (Fig. 7 b) and d)-g)) and the chloride diffusion coefficients (Fig. 5) that chloride diffusion decreases with depth due to the decrease in moisture content. Another factor that contributes to the convex shape is the non-linearity of the chloride binding isotherms [21]. At saturated conditions, it is generally observed that chloride binding is non-linearly related to chloride concentration in the pore solution, and that

binding capacity decreases with increase in concentration [22, 23]. However, there is a lack of knowledge on how chloride binding is affected at low moisture content and RH in the pore structure [24]. If chloride binding in unsaturated condition behaves in a similar way to that in a saturated system, then this would contribute to the convex shape seen in Fig. 1 b)-d).

Coupled transport of ions and moisture is a complex phenomenon that needs further research in order to be fully clarified. There is a general lack of knowledge on the interaction between the ions in pore solution and the solid phases at unsaturated conditions, i.e. the ion binding isotherms at unsaturated conditions. There is also a need for clarification of the interaction between water activity, degree of saturation and ionic strength, i.e. the sorption isotherms at different ionic strengths.

5 Conclusions

The most important observations in the study of wick action exposure can be summarized as follows:

- For plain OPC mortars, chlorides have penetrated through specimen thickness (35 mm) and begun to accumulate near the surface exposed to lower RH. The amount of chloride ingress and accumulation increased with increase in w/b and drying severity. Convective transport of ions with moisture transport is the dominant mechanism in these OPC systems which have larger moisture transport compared to the other systems in this study.
- In contrast, mortars containing SCMs showed much smaller chloride penetration depths and no significant accumulation near the surface exposed to lower RH. Under

the given experimental conditions, mortars with 70% slag gave the highest resistance to chloride ingress, followed by 40% slag and 5% SF, regardless of w/b and drying humidity. The 70% slag mortars also showed the greatest chloride binding capacity.

- The chloride diffusion coefficient, moisture diffusion coefficient and chloride binding properties are important parameters for the prediction of chloride ingress during wick action exposure. All of these parameters are also strongly related to the cementitious binder and are moisture dependent in some cases.
- The moisture dependency of the moisture diffusion coefficient is an important factor influencing chloride penetration in porous materials where ion transport occurs predominantly by convection. But for denser materials with little or no moisture transport, such as systems containing SCMs, the limited moisture transport contributes to the high resistance to chloride ingress. In these systems, the diffusive ion transport and its moisture dependency needs to be considered for accurate assessment of chloride penetration. Additionally, the enhanced chloride binding capacity in systems containing SCMs, is another key factor limiting chloride penetrations depth.
- There is still a lack of knowledge about the interaction between the ions in pore solution and the solid phases in unsaturated conditions.
- Even though it is outside the scope of this publication, it needs to be pointed out that quantitative evaluation of moisture content profiles in cementitious materials from NMR-measurements needs extensive calibration due to the differences in sensitivity to water in different pore sizes.

The results presented in this paper constitute valuable data for the development of mass transport models for cementitious systems containing SCMs in non-saturated conditions. The

results also contribute new understanding of the key parameters influencing chloride penetration, which can be used for the development of new binders.

Acknowledgements

The authors are grateful to Nanocem for funding the project. SBUF (Development Fund of the Swedish Construction Industry) and NCC AB are acknowledged for additional funding during the last year of the project. The authors are also grateful to Bo Johansson at Lund University, Francois Marin-Cudraz and Andrew Morris at Imperial College, and co-workers at Technical University of Munich for their kind assistance with the experiments.

References

[1] L.-O. Nilsson, On the role of moisture in degradation of concrete structures, in: R.K. Dhir, M.R. Jones, L. Zheng (Eds.) International Congress - Global Construction: Ultimate Concrete Opportunities Dundee, Scotland, United Kingdom, 2005, pp. 15-24.
[2] N.R. Buenfeld, M.-T. Shurafa, I.M. McLoughlin, Chloride transport due to wick action in concrete, in: L.-O. Nilsson, J.P. Ollivier (Eds.) Int. RILEM workshop "Chloride penetration into concrete" St-Remy-les-Chevreuse, France, 1995, pp. 315-324.
[3] V. Baroghel-Bouny, M. Thiéry, X. Wang, Modelling of isothermal coupled moisture-ion transport in cementitious materials, Cement and Concrete Research, 41 (2011) 828-841.
[4] E. Samson, J. Marchand, K.A. Snyder, J.J. Beaudoin, Modeling ion and fluid transport in unsaturated cement systems in isothermal conditions, Cement and Concrete Research, 35 (2005) 141-153.
[5] O. Francy, Modélisation de la pénétration des ions chlorures dans les mortier partiellement saturés en eau, LMDC, Univeristé Paul Sabatier, Toulouse 1998, pp. 171.
[6] N. Olsson, L.-O. Nilsson, M. Åhs, V. Baroghel-Bouny, Moisture transport and sorption in cement based materials containing slag or silica fume, Cement and Concrete Research, 106 (2018) 23-32.
[7] K. Tuutti, Corrosion of steel in concrete, Ph.D Thesis, Report fo 4-82. Swedish Cement and Concrete Research Institute, Stockholm, Sweden, 1982.
[8] Y. Zhang, M. Zhang, Transport properties in unsaturated cement-based materials – A review, Construction and Building Materials, 72 (2014) 367-379.
[9] N. Olsson, B. Lothenbach, V. Baroghel-Bouny, L.-O. Nilsson, Unsaturated ion diffusion in cementitious materials – The effect of slag and silica fume, Cement and Concrete Research, 108 (2018) 31-37.

[10] N. Olsson, V. Baroghel-Bouny, L.-O. Nilsson, M. Thiery, Non-saturated ion diffusion in concrete – A new approach to evaluate conductivity measurements, Cement and Concrete Composites, 40 (2013) 40-47.
[11] L. Greenspan, Humidity fixed points of binary saturated aqueous solutions J Res Natl Bur Stand Sect A Phys Chem, 81 A (1977) 89-96.
[12] F. Abdul Wahid, Characterising concrete using micro X-ray fluorescence (μXRF), PhD thesis, Imperial College London, 2017.
[13] F. Marin-Cudraz, Characterising non-saturated transport in mortars using micro X-ray fluorescence, Department of Civil and Environmental Engineering, Imperial College, London 2015.
[14] B. Blümich, P. Blümler, G. Eidmann, A. Guthausen, R. Haken, U. Schmitz, K. Saito, G. Zimmer, The NMR-mouse: construction, excitation, and applications, Magnetic Resonance Imaging, 16 479-484.
[15] C. Thiel, C. Gehlen, Nuclear magnetic resonance (NMR) and Magnetic Resonance Imaging (MRI), in: L.-O. Nilsson (Ed.) Methods of measuring moisture in building materials and structures - State-of-the-art report of the RILEM Technical Committee 248-MMB, To be published by Springer early 2018.
[16] H.S. Wong, A.M. Pappas, R.W. Zimmerman, N.R. Buenfeld, Effect of entrained air voids on the microstructure and mass transport properties of concrete, Cement and Concrete Research, 41 (2011) 1067-1077.
[17] Z. Wu, H.S. Wong, N.R. Buenfeld, Transport properties of concrete after drying-wetting regimes to elucidate the effects of moisture content, hysteresis and microcracking, Cement and Concrete Research, 98 (2017) 136-154.
[18] S.D. Abyaneh, H.S. Wong, N.R. Buenfeld, Simulating the effect of microcracks on the diffusivity and permeability of concrete using a three-dimensional model, Computational Materials Science, 119 (2016) 130-143.
[19] P. Rucker-Gramm, Modellierung des Feuchte- und Salztransports unter Berücksichtigung der Selbstabdichtung in zementgebundenen Baustoffen (in German) Technical University of Munich, Munich, Germany 2008.
[20] H. Garrecht, H.K. Hilsdorf, J. Kropp, Hygroscopic salt influence on the moisture behaviour of structural elements, in: J.M. Baker (Ed.) Durability of Building Materials and Components: Proceedings of the Fifth International Conference Held in Brighton, UK, 7-9 November 1990.
[21] L.-O. Nilsson, M. Massat, L. Tang, The effect of non-linear chloride binding on the prediction of chloride penetration into concrete structures, Contribution to the 3rd CANMET/ACI International Conference on Durability of Concrete, Nice, France, 22-28 May 1994; also in: Malhotra (Ed.) (1994) Durability of Concrete, ACI SP 145-24, pp. 469- 486., 1994.
[22] V. Baroghel-Bouny, X. Wang, M. Thiery, M. Saillio, F. Barberon, Prediction of chloride binding isotherms of cementitious materials by analytical model or numerical inverse analysis, Cement and Concrete Research, 42 (2012) 1207-1224.
[23] L. Tang, L.-O. Nilsson, M. Basheer, Resistance of concrete to chloride ingress: Testing and modelling, Taylor and Francis2012.
[24] C.K. Larsen, Chloride binding in concrete: effect of surrounding environment and concrete composition, Norwegian University of Science and Technology, Department of Structural Engineering, Trondheim, 1998, pp. XX, 325 s. ill.

608 Table 1
609 Composition of mortars.

Mortar label	OPC 0.38	5% SF 0.38	40% slag 0.38	70% slag 0.38	OPC 0.53	5% SF 0.53	40% slag 0.53	70% slag 0.53
Cement/SCM w/b	100/0 0.380	95/5 0.381	60/40 0.391	30/70 0.386	100/0 0.530	95/5 0.531	60/40 0.539	30/70 0.545
CEM 1 (kg/m^3)	516	509	308	153	436	427	260	129
Slag (kg/m^3)	-	-	206	357	-	-	174	302
Silica Fume (kg/m^3)	-	27	-	-	-	23	-	-
Water (kg/m^3)	196	204	198	200	231	239	234	235
Normsand (kg/m^3)	1548	1607	1543	1531	1525	1574	1519	1508
Plastisizer (kg/m^3)	1.18	1.06	0.94	0.96	-	-	-	-
Density (kg/m^3)	2256	2253	2236	2208	2198	2203	2199	2201

610

611 Table 2
612 Composition of a) OPC b) slag and c) SF.

613 a)

Chemical Analysis XRF	
	g/100g
SiO_2	19.88
Al_2O_3	4.47
Fe_2O_3	3.96
CaO	63.49
MgO	1.77
K_2O	0.86
Na_2O	0.17
TiO_2	0.32
Mn_2O_3	0.05
P_2O_5	0.22
SrO	0.05
Cl	0.03
F	<0.1
ZnO	0.02
Cr_2O_3	0.01
SO_3	2.96

Mineralogical Composition - XRD/Rietveld analysis	
	g/100g
Alite	66.7
Belite	8.4
Aluminate	6.2
Ferrite	9.6
Arcanite	1.6
Free Lime	0.1
Portlandite	0.5
Periclase	0.5
Gypsum	1.2
Hemihydrate	2.2
Calcite	3.1
Anhydrite	0.1

b)

Chemical Analysis -XRF	
	g/100g
SiO_2	36.11
Al_2O_3	9.97
Fe_2O_3	0.43
CaO	42.25
MgO	7.26
K_2O	0.41
Na_2O	0.28
TiO_2	0.61
Mn_2O_3	0.35
P_2O_5	0.01
SrO	0.07
BaO	0.08
Cl	<0.005
F	<0.1
SO_3	3.3

Mineralogical Composition - XRD/Rietveld analysis	
	g/100g
Amorphous	96.7
Gypsum	2.3
Anhydrite	0.2
Merwinite	0.8

614 c)

Chemical Analysis XRF	
	g/100g
SiO_2	98.7
Al_2O_3	0.3
Fe_2O_3	0.02
CaO	0.15
MgO	0.04
K_2O	0.3
Na_2O	0.09
TiO_2	0.39
Mn_2O_3	0.01

P_2O_5	0.02

615

616 a)

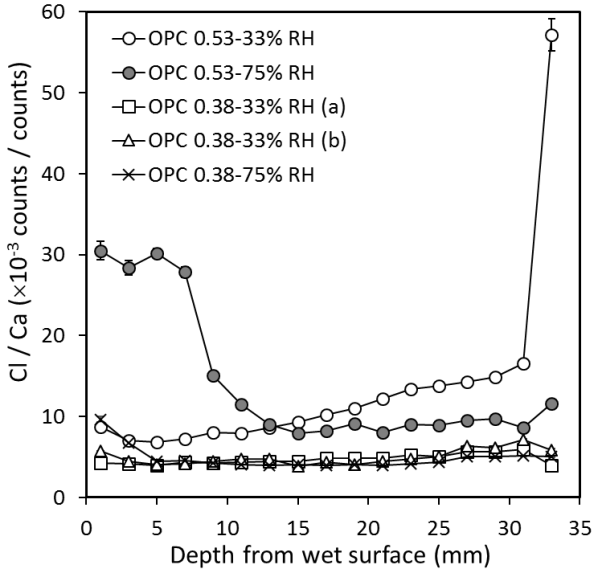

617

618 b)

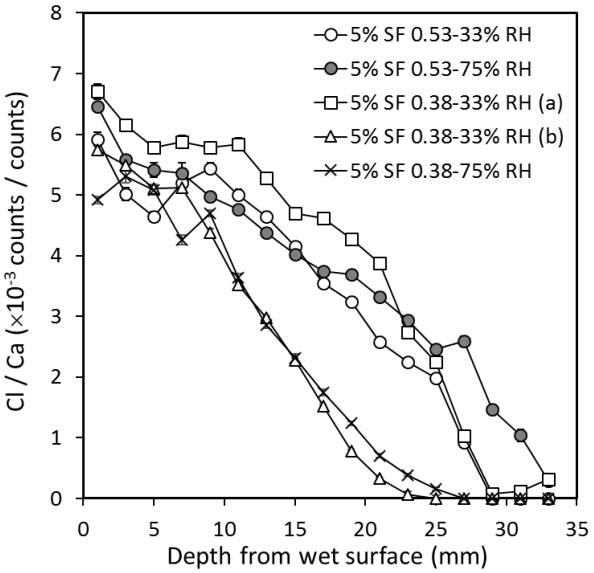

619

620 c)

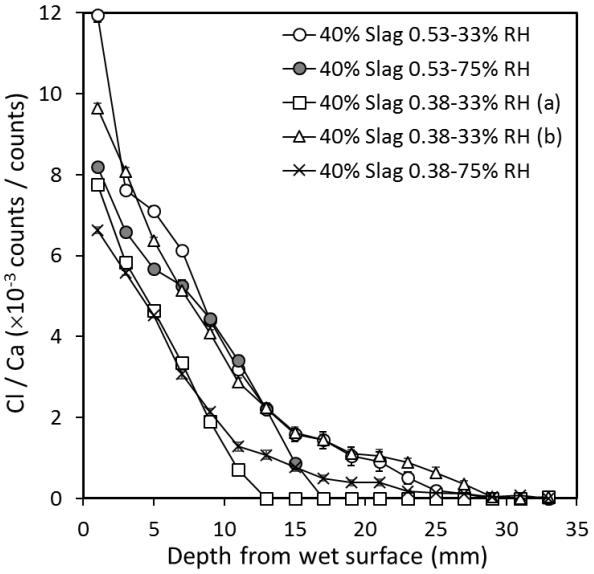

d)

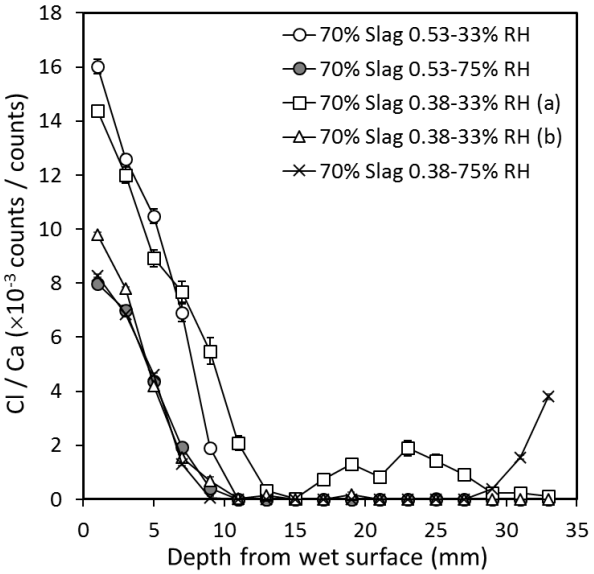

Fig. 1. Chloride profiles for a) OPC, b) 5% SF, c) 40% slag, and d) 70% slag mortars. Specimens were exposed to NaCl solution at 0 mm and drying at controlled RH (75% or 33%) at 35 mm for 30 months prior to measurements. Significant differences in penetration depths were observed between the four binders.

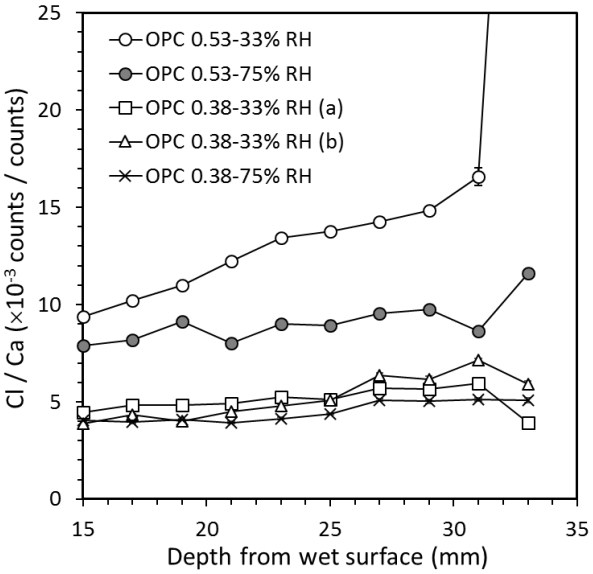

629

630 Fig. 2. Detail from Fig. 1a showing the chloride profiles for OPC mortars near the drying side
631 of specimen. Accumulation of chlorides increased with increase in w/b ratio and drying
632 severity.

633

634 a)

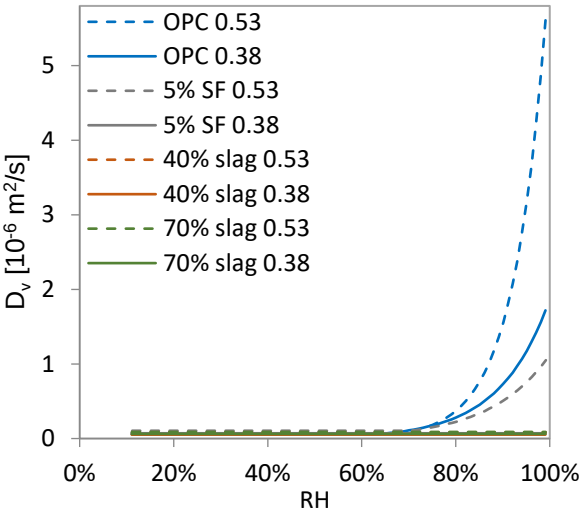

635

636 b)

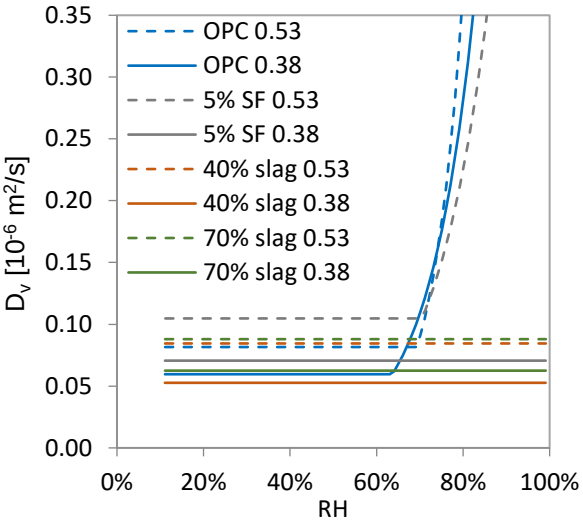

Fig. 3. a)-b) Moisture diffusion coefficients for all mortars, D_v, adopted from [6]. Three mortars have a clear moisture dependency in the moisture diffusion coefficient at RH from 70% to 100% RH. The other five mortars have no moisture dependency in the diffusion coefficient in this range of RH. This yields large differences in moisture transport. (For interpretation of the color in this figure, the reader is referred to the web version of this article.)

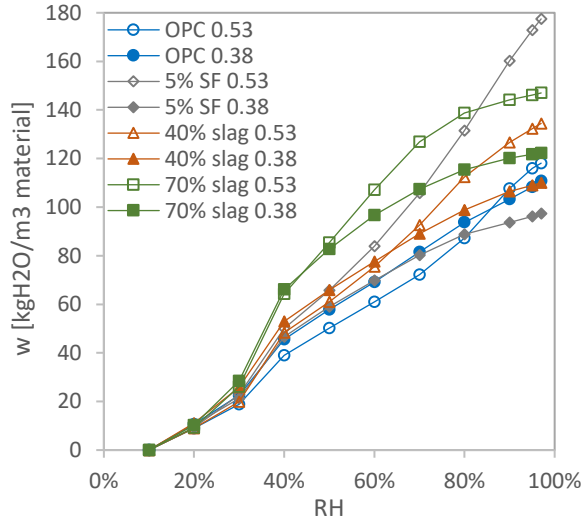

Fig. 4. Desorption isotherms for all mortars adopted from [6]. The amount of moisture is of the same order of magnitude for all mortars. However looking at specific RH ranges, differences can be observed e.g. in the RH range from 75% to 97% RH.

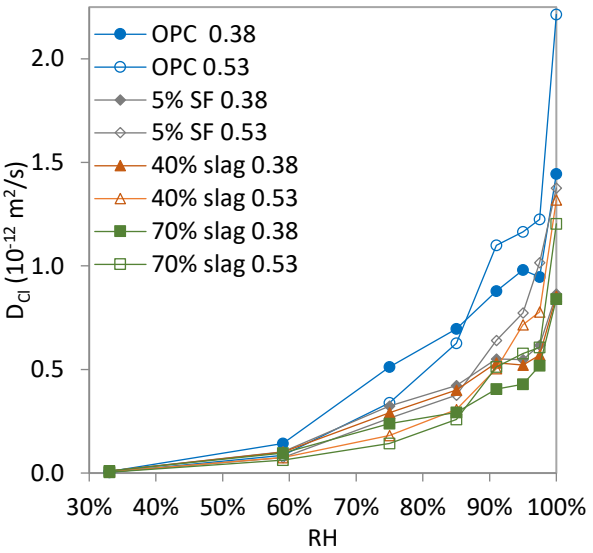

Fig. 5. Chloride diffusion coefficient for all mortars, D_{Cl}, adopted from [9]. All mortars show the same behavior with a clear moisture dependency in the chloride diffusion coefficient.

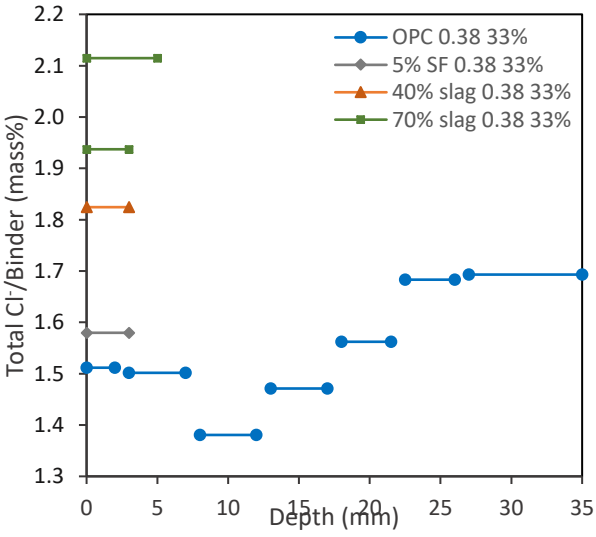

Fig. 6. Measured total chloride content for selected depth intervals and specimens. The results represent the average chloride content in the interval on the x-axis. The total chloride content at 0 mm gives an indication of the difference in chloride binding between the binders. The total chloride content is shown for all depths for the OPC binder. The profile correlates well with the same profile measured with microXRF.

a)

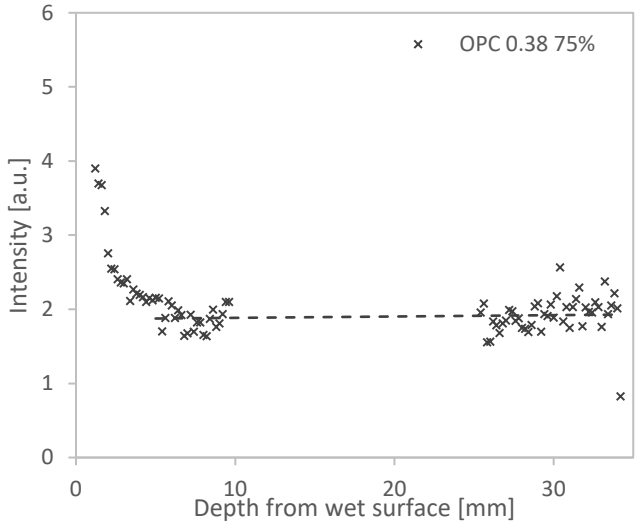
OPC 0.38 75%
Intensity [a.u.]
Depth from wet surface [mm]
0
1
2
3
4
5
6
0
10
20
30

b)

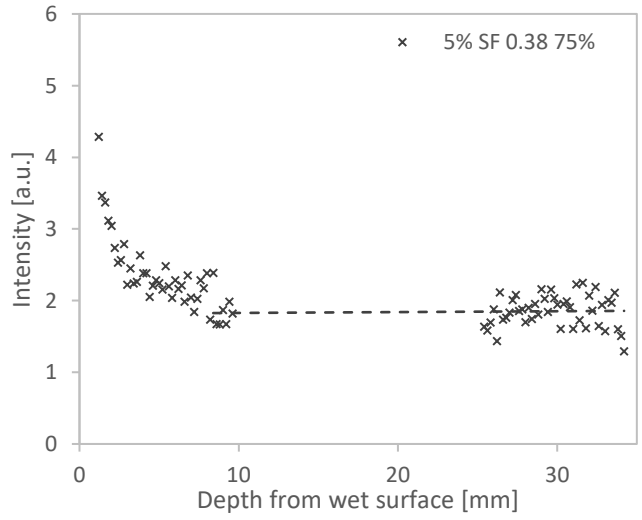
5% SF 0.38 75%
Intensity [a.u.]
Depth from wet surface [mm]
0
1
2
3
4
5
6
0
10
20
30

c)

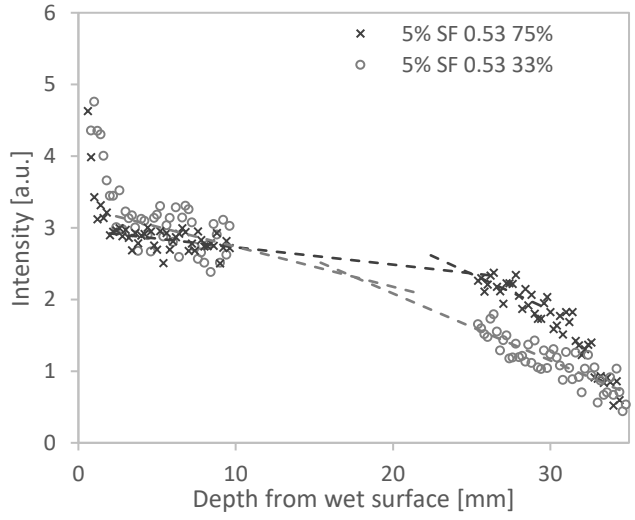
5% SF 0.53 75%
5% SF 0.53 33%
Intensity [a.u.]
Depth from wet surface [mm]
0
1
2
3
4
5
6
0
10
20
30

d)

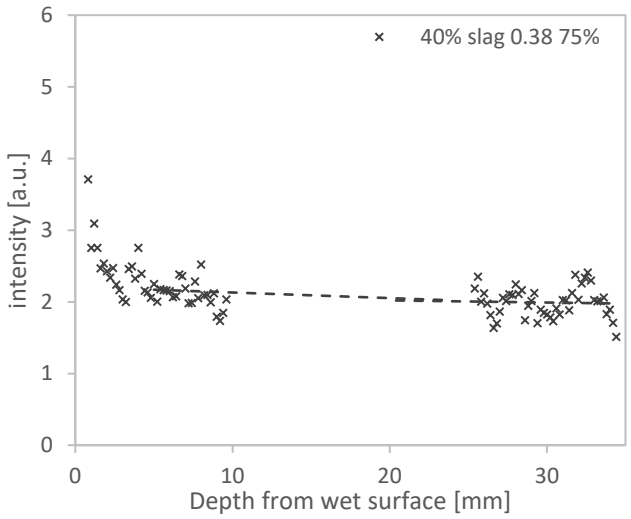
40% slag 0.38 75%
intensity [a.u.]
Depth from wet surface [mm]

e)

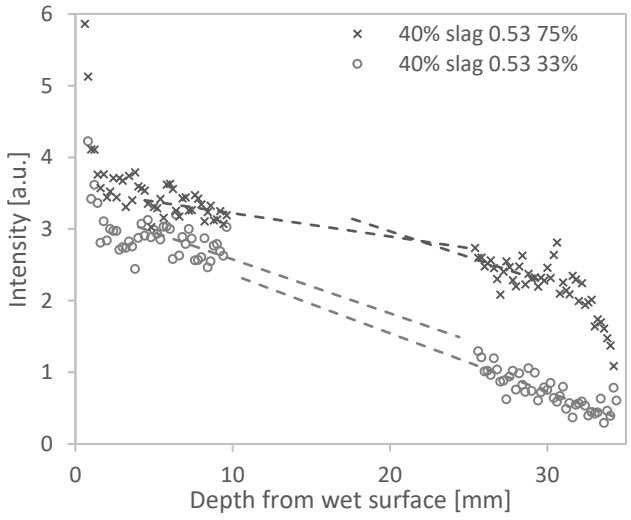
40% slag 0.53 75%
40% slag 0.53 33%
Intensity [a.u.]
Depth from wet surface [mm]

f)

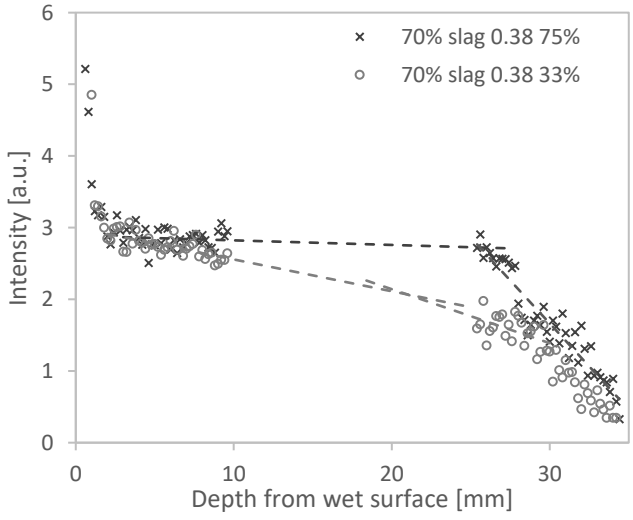
70% slag 0.38 75%
70% slag 0.38 33%
Intensity [a.u.]
Depth from wet surface [mm]

678 g)

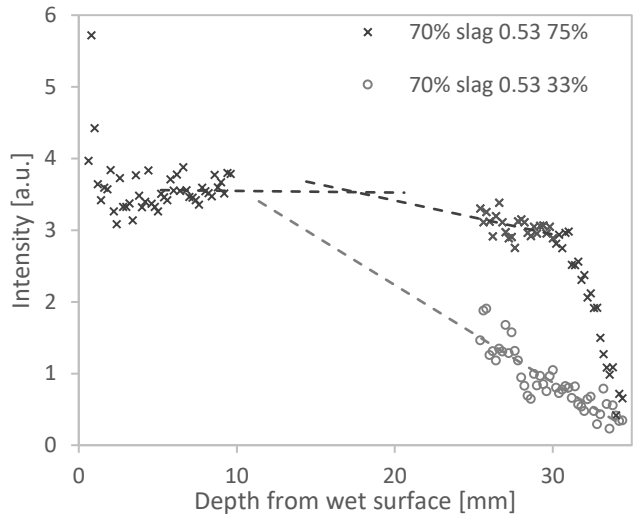

679

680 Fig. 7. Moisture profiles for a) OPC 0.38 - 75% RH, b) 5% SF 0.38 - 75% RH, c) 5% SF 0.53
681 - 33% and 75% RH, d) 40% slag 0.38 - 33% and 75% RH, e) 40% slag 0.53 - 33% and 75%
682 RH, f) 70% slag 0.38 - 33% and 75% RH, and g) 70% slag 0.53 - 33% and 75% RH.

683

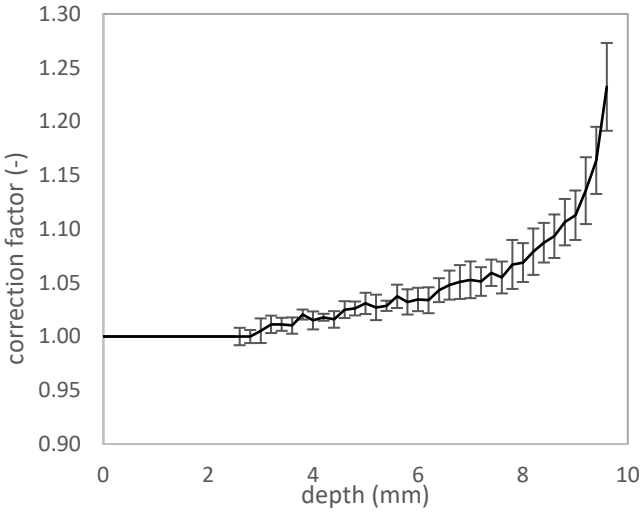

684

685 Fig. 8. Correction factor to account for the decrease in measured NMR signal amplitude with
686 increase in sample depth. The error bars represent standard errors.

687

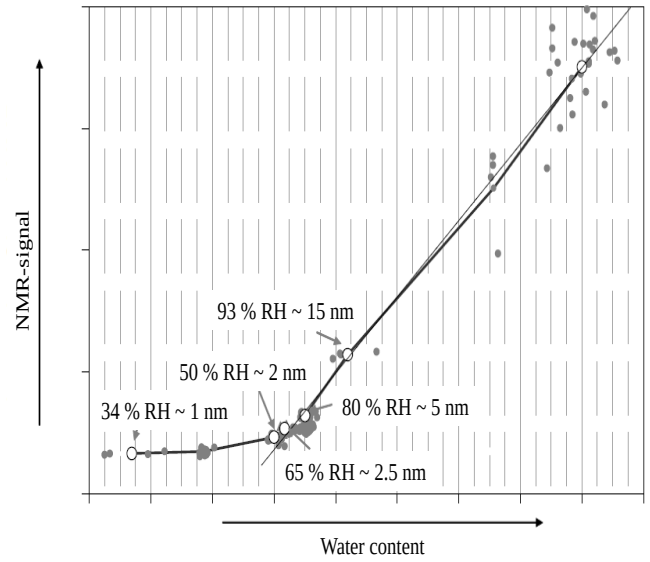

688

689 Fig. 9. Relation between NMR-signal and water content adopted from [14] and based on data
690 from [18].

691

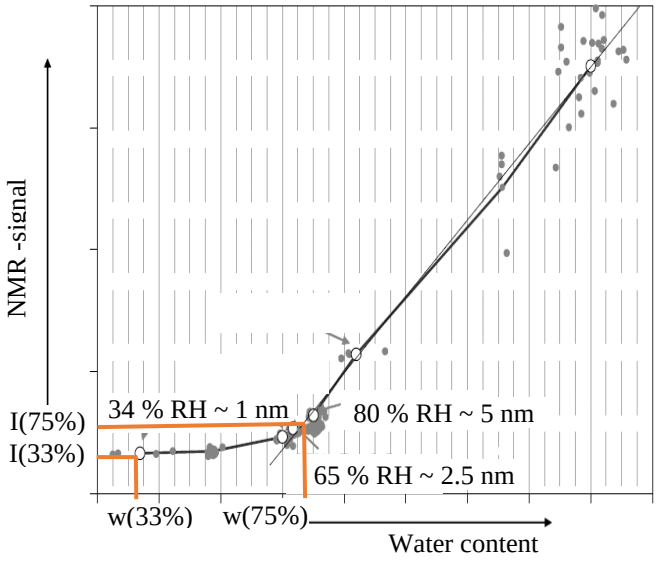

692 Fig. 10. Interpretation of the measured NMR-signal intensity in terms of moisture content.
693 The relation between NMR-signal and water content [14] with relevant values marked.

694

695

696

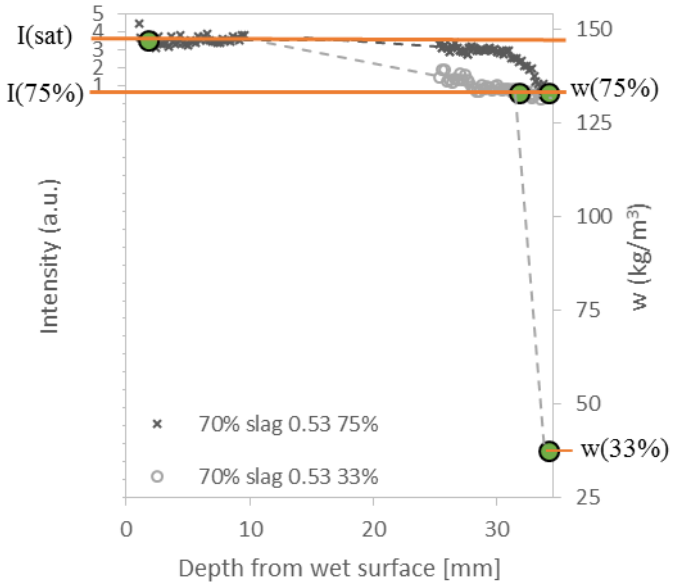

Fig. 11. Interpretation of the measured NMR-signal intensity in terms of moisture content. The results in Fig. 7 h) with an axis for moisture content, and relevant values from Fig. 10 marked. The absolute values in moisture content are taken from Fig. 4. The effect of the non-linear relation between measured NMR-signal intensity and water content is demonstrated.